JOURNAL OF PROPULSION AND POWER
Vol. 17, No. 1, January–February 2001

Origins of Accelerator Grid Current: Analysis of T5 Grid Test Results

Mark W. Crofton*
The Aerospace Corporation, El Segundo, California 90245-4691
and
Iain D. Boyd†
University of Michigan, Ann Arbor, Michigan 48109-2140

Grid-current levels were obtained at various operating points of a T5 ion thruster using flight-model extraction grids. Because of the improved grid design and precision fabrication, better analysis of the dependence of grid current on operating point could be performed. The decelerator current can be interpreted in terms of impingement by charge exchange ions, although the dependence on operating point is not simple. The accelerator grid current was found to have a major component that appears to be independent of charge exchange. A direct simulation Monte Carlo–particle-in-cell model was constructed that includes the effects of momentum transfer, ion-neutral charge exchange, coulomb collisions, and double-charge ions. Through the use of existing far-field data on the energy distribution of beam ions, good relative and absolute agreement between theory and experiment has been achieved. The results suggest a new erosion mechanism that depends on ion radial velocity distribution during extraction. Ions with high radial velocity have relatively high probability of impinging on the accelerator grid and will do so with larger sputter yield than charge exchange ions. Double-charge ions have a lower impingement probability. The results have implications for the lifetime and contamination effects of ion thrusters using extraction grids.

Nomenclature

C	=	mean molecular speed
E	=	kinetic energy
e	=	elementary unit of charge, coulomb
F	=	propellant mass flow rate through grids, mg/s
F_0	=	mass flow rate of neutral xenon through grids, mg/s
f_{2+}	=	Xe^{2+} fractional current
g	=	relative velocity
I_{acc}	=	total accelerator grid current, mA
I_{acc}^E	=	accelerator current due to charge exchange, mA
I_{beam}	=	beam current, mA
I_{dec}	=	decelerator grid current, mA
k	=	Boltzmann constant
m	=	particle mass, g
n_e	=	electron density
n_{ref}	=	reference plasma density
T	=	temperature, K
T_e	=	electron temperature, eV
V_{acc}	=	accelerator grid voltage
V_{anode}	=	anode to cathode voltage of discharge chamber
V_{beam}	=	ion beam voltage, V_{anode} relative to absolute ground
V_{dec}	=	decelerator grid voltage
Γ	=	particle flux
η_c	=	propellant mass utilization, corrected
η_m	=	propellant mass utilization
σ	=	reaction cross section
ϕ	=	local plasma potential, V
ϕ_0	=	bulk plasma potential in the discharge, V
χ	=	coulomb collision scattering angle, deg

Presented as Paper 99-2443 at the AIAA/ASME/SAE/ASEE 35th Joint Propulsion Conference and Exhibit, Los Angeles, CA, 20–24 June 1999; received 13 September 1999; revision received 8 January 2000; accepted for publication 16 January 2000.

*Research Scientist, 2350 E. El Segundo, Boulevard, Space Materials Laboratory, M5-754. Member AIAA.

†Associate Professor, Department of Aerospace Engineering, 1320 Beal Avenue. Member AIAA.

Introduction

FOR ion engines, erosion of the accelerator grid is a principal life-limiting process and a primary source of thruster-induced spacecraft contamination (Refs. 1 and 2 and the references therein and Refs. 3 and 4). The usual grid material, molybdenum, is sputtered into the ion engine plume. It deposits on neighboring surfaces on contact, leaving a metallic coating that alters surface properties and may affect the performance of solar arrays, sensors, and thermal control materials.

The limitation of lifetime due to accelerator grid erosion exerts considerable influence on the choice of thruster type and rated thrust for spacecraft. The end of life is usually taken at the point of grid mechanical failure due to extensive loss of the webbing. This results in the loss of beam current capability and the onset of electron backstreaming into the discharge chamber. The erosion of grid material may also produce flakes, which electrically short adjacent grids, causing premature failure unless the short can be cleared. For the more than 60 ion-engine endurance tests that have been reported, the majority of failure modes involved the accelerator grid.[1] To partially mitigate grid erosion effects, significant effort has been expended in the development of grids using erosion-resistant materials (Refs. 5 and the references therein and Ref. 6).

Many studies have been devoted to the subject of accelerator grid wear (for recent examples, see Refs. 7 and 8). During the past decades of ion-engine research and development, the impingement of charge exchange (CEX) ions has been accepted as the cause of the erosion under normal operating conditions. It has been recognized that under special circumstances, such as when the perveance limit is exceeded, the grids are poorly designed, or grid apertures are misaligned, direct impingement of ions at the ion beam energy or above may occur. These energetic ions have a far higher sputter yield than CEX ions,[9] which, with a typical −200 or −300 V on the accelerator, impinge at a relatively low energy.

The impingement rate of CEX ions increases with background pressure, necessitating the use of high pumping speeds during testing. Reduction of the accelerator grid erosion rate is also achieved by incorporating a negatively biased decelerator grid and operating the accelerator grid at a negative potential of low absolute value to limit the sputtering yield.[10]

Considerable evidence exists that the impingement of CEX ions may not be the only cause of accelerator grid erosion under normal operating conditions. Several measurements on the T5 ion thruster, which has been extensively studied,[2] have shown that the accelerator grid current and erosion rate is far from zero when the utilization of xenon propellant is extrapolated to 100%.

One of these measurements consisted of directly monitoring the laser-induced-fluorescence signal from T5 plume molybdenum atoms as a function of η_m (Ref. 11). A second monitored the rate of mass gain, largely from molybdenum, at a quartz crystal microbalance (QCM) as a function of η_m, obtaining a similar curve.[12] The rate of mass gain as a function of background pressure further demonstrated that the grid erosion was only slightly affected by CEX in the background gas.[12] The accelerator current exhibited similar dependence as the mass gain, whereas decelerator-current percentage variation was much higher. All of these results taken together suggested that CEX ion impingement did not fully account for I_{acc} at the higher η_m operating points. However, design and fabrication flaws of the triple grid set used in these studies [baseline triple grid set (BTS)], and the known presence of decelerator direct impingement presented a limitation to any attempt to elucidate a secondary erosion mechanism. The flight-quality grids used in the present study were needed to address the issue.

Several studies have compared the accelerator mass loss over an extended period of operation with its calculated loss. The comparisons, based on current collection and the sputter coefficient for an assumed impingement energy of CEX ions, have frequently obtained puzzling results.[7,13]

Experimental

Details of the facility have been described previously.[2] The test chamber is 5.5 m in length and 2.4 m in diameter. Two custom reentrant cryopumps of combined ≈70,000 l/s pumping speed on xenon hang inside the chamber, suspended from flanges. During thruster operation at a nominal thrust level of 18 mN, the chamber pressure was determined to be 1.5×10^{-6} torr, after applying a standard xenon-sensitivity correction to the indicated ion gauge reading.

The thruster was mounted on a fixed stand in a side chamber with the ion beam directed across the main chamber. The beam dump consisted of aluminum plates covered with carbon–carbon composite panels, without water cooling.

In the present study, two extraction grid sets of flight quality (designated 003 and 004) were installed on the T5 ion thruster already characterized by past studies,[2] to perform design validation. Each grid set was subjected to a wear test of approximately 50 h in duration.

The thruster is diagrammed in Fig. 1. The anode was biased at the usual 1100-V operating point.[2] The screen grid and discharge chamber wall were about 40 V lower according to the value of the discharge voltage.

The grid sets were manufactured to identical specifications. The screen and decelerator apertures were 2.15–2.18 mm in diameter, with a hole pitch of about 2.44 mm. The accelerator aperture diameter was 1.75–1.78 mm with similar pitch. Grids were 0.25 mm thick for screen and decelerator grids and 1.00 mm for the accelerator grid, which was spaced 0.75 mm from the screen grid and 0.50 mm from the decelerator grid. Alignment and concentricity of grid set

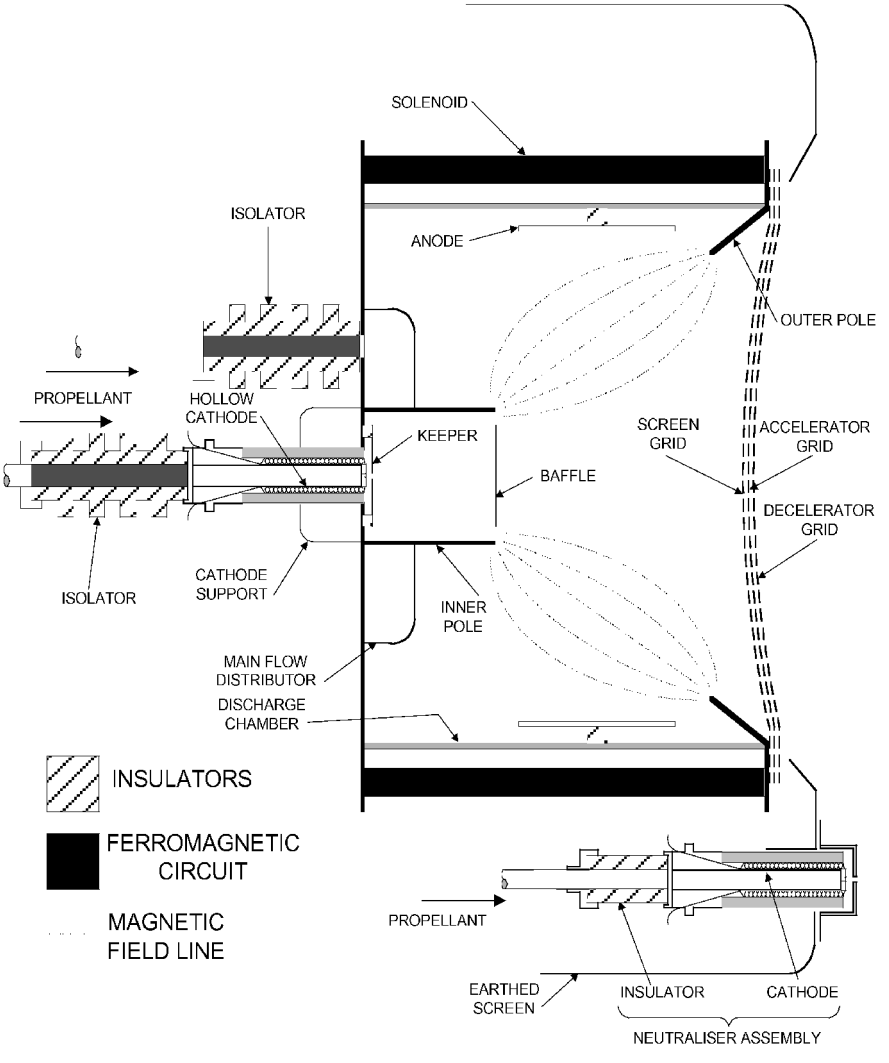

Fig. 1 Schematic of T5 ion thruster.

(GS)003 and GS004 were perfect to the naked eye, and far better than for the BTS grids.

GS003 had been previously operated for a period of roughly 50 h at thrust levels $\leq$18 mN. There were no prior hours of operation on GS004. The performance of the GS varied slightly at $\leq$22 mN, with GS003 generally collecting a bit less accelerator current at a given operating point. This can be attributed to its prior period of operation.

The critical parameter of propellant utilization efficiency, η_m, was determined from calibrations of shunted flow rates with engine off, monitoring the rate of pressure rise in a known volume. The ratio of I_{beam} to the electrical-current equivalent of the propellant flow rate was computed, assuming no multiple-charge states. The absolute accuracy is better than $\pm 2\%$ in each case. No correction to η_m was made for multiply charged ions because only approximate values for the charge state ratios were available over the range of operating points. Neutralizer flow was not included in the calculation of η_m, because discharge chamber utilization was the relevant parameter rather than overall engine utilization. It was assumed that the flow rates measured with the engine off were identical to those obtained with the engine on.

Experimental Results and Analysis

Performance of GS003

The observed thruster performance at several operating points is shown in Table 1. Previous performance figures obtained on the triple GS (BTS) used during the extensive prior characterization of the T5 (Ref. 2) are given in Table 1 for comparison. Accelerator grid currents at the nominal 18-mN thrust level are similar in the two cases, although it appears to be about 10% higher for GS003 at 18 mN and mass utilization near 85%. Decelerator grid current level was about 45% lower for GS003 than for the BTS grid for the same 18-mN operating points. The deposition rate measured by a QCM indicated that GS003 eroded much less rapidly than BTS; GS003 deposition rate was about 50% less, and so its grid erosion rate would be less by at least that amount.[12] Because the accelerator current of the two GSs was similar, it appears that the reduced deposition rate could be explained by a reduction in GS003 decelerator-grid erosion rate. The presence of direct impingement on the BTS decelerator grid had been documented previously.[12] The major differences between the grid sets were 1) decelerator grid thickness of 0.25 mm for GS003 vs 0.75 mm for BTS and 2) better aperture alignment and more uniform grid spacing for GS003. Both factors are qualitatively consistent with a substantial reduction in direct impingement by ions with energies determined by the full-voltage difference between screen and decelerator grids.

The propellant mass utilization efficiency, η_m, is given by $(I_{\text{beam}}/F)(m/e)$ and is valid if the only charge state is $+1$. The presence of the $+2$ charge state cannot be ignored in the present situation. We define the corrected utilization, η_c, as $(1 - F_0/F)$. Neglecting all charge states except 0, $+1$, and $+2$, the result is $\eta_c = (1 - 0.5 f_{2+})\eta_m$. The fractional Xe^{2+} current was estimated from Pollard's data,[14] and the resulting values of η_c are included in Table 1. For the source flow, the density of neutral xenon in the intergrid region and downstream is proportional to $(1 - \eta_c)F$, and its product with I_{beam} is a measure of the total rate of CEX ion production. The proportionality constant was designated P_E.

A secondary contribution to the CEX current stems from the background density of neutral xenon in the test chamber. The base pressure of the vacuum pumps is much lower than the background pressure during thruster operation, and the term is proportional to $F I_{\text{beam}}$. The proportionality constant was designated P_{EB}.

To perform least squares fitting of the grid current data, additional terms in I_{beam} and its square were included. With these terms, and a constant offset term, there were five parameters included in the initial fits to I_{acc} and I_{dec}, according to the expression

$$I = (1 - \eta_c)F(1 - f_{2+}/2)(I_{\text{beam}}/329)P_E + (1 - f_{2+}/2) \times (I_{\text{beam}}/329)P_I + (1 - f_{2+}/2)(I_{\text{beam}}/329)^2 P_{I2} + F(1 - f_{2+}/2)(I_{\text{beam}}/329)P_{\text{EB}} + C \quad (1)$$

The functional forms of the P_E and P_{EB} terms were obtained from first principles, but the remaining terms were chosen to improve the quality of the fit. The inclusion of $(1 - 0.5 f_{2+})$, a correction factor applied to I_{beam} wherever it appears, is equivalent to the assumption that Xe^{2+} ions have the same effect on impingement current as Xe^{+} on a per particle basis rather than per unit of charge.

When a parameter was found to make little difference to the quality of a fit it was eliminated. In the case of I_{dec}, a good fit required a minimum of three parameters. The 3-parameter fit judged to give the best results included the P_E term as the dominant contributor, plus the P_I and P_{I2} terms. The result is indicated in Fig. 2 and Table 2. The maximum residual was $>30\,\mu$A. The source CEX term accounted for an impingement current higher than the observed I_{dec} at most operating points. There are two operating points in Table 1 with similar I_{beam}. Scaling $I_{\text{dec}} = 0.46$ mA of case (4) according to $(1 - \eta_c)F(1 - 0.5 f_{2+})I_{\text{beam}}$ produces $I_{\text{dec}} = 0.70$ mA, just 10 μA higher than the observed level of case (3). This result and the fit itself provide strong evidence that the decelerator current is primarily due to impingement of CEX ions, of which little is associated with the background gas.

The contributions of P_I and P_{I2} terms were positive and negative, respectively, and their sum makes a small, negative correction (the P_{I2} term is not shown in Fig. 2). It seems inevitable that CEX ions formed downstream will not have quite the same probability of decelerator capture at different I_{beam} settings. This probability depends on the electric potential in the plume, since the potential distribution determines the trajectories for CEX ions. According to the limited data available, the plume plasma potential exhibits a slow increase

Table 2 Parameter coefficients determined by least squares fitting of grid current data

	T5 decelerator fit		T5 accelerator fit		NSTAR accelerator fit	
Coefficient	Value	Std. dev.	Value	Std. dev.	Value	Std. dev.
P_E	4.117	0.30	5.415	0.43	−1.823	2.81
P_{EB}						
P_I	0.344	0.067	0.441	0.062	0.073	0.44
P_{I2}	−0.445	0.066			0.483	0.29

Table 1 Operating parameters for selected operating points, GS003[a]

Case	Operating point	I_{beam}, mA	V_{anode}, V	I_{anode}, A	I_{acc},[b] mA	I_{dec},[b] mA	$I_{\text{acc}} + I_{\text{dec}}$, mA	η_m, %	η_c, %	F, mg/s
1	11.9 mN	218	44.8	1.50	0.53	0.25	0.78	82.4	75.4	0.359
2	14.8	270	40.8	1.85	0.90	0.44	1.34	76.2	72.0	0.482
3	17.9	327	37.2	2.90	1.43	0.69	2.12	71.0	68.5	0.626
4	17.9	328	40.7	2.50	1.10	0.46	1.56	81.0	75.9	0.551
5	19.0	348	43.0	——	1.05	0.38	1.43	85.9	79.0	0.551
6	19.9	363	38.9	2.90	1.37	0.55	1.92	78.8	75.1	0.626
7	21.8	399	43.0	2.90	1.25	0.40	1.65	86.7	79.8	0.626
8	18.0 (BTS)	329	43.0	2.25	0.90	0.65	1.55	85.6	79.0	——

[a] $V_{\text{beam}} = 1100$ V, $V_{\text{acc}} = -225$ V, and $V_{\text{dec}} = -50$ V. [b] Absolute accuracy is $\pm 10\,\mu$A.

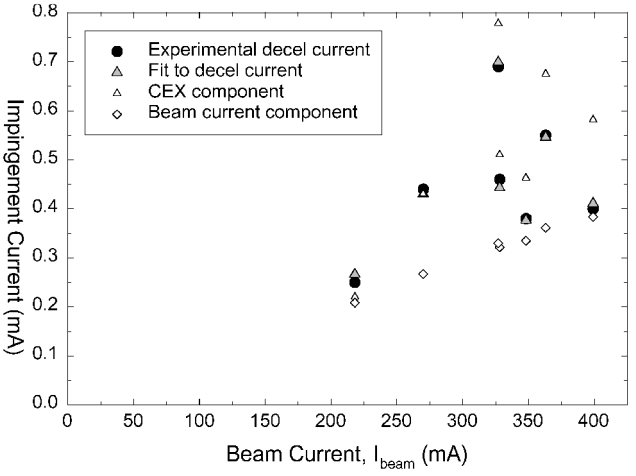

Fig. 2 Observed decelerator grid current for GS003 and results of the least squares fit.

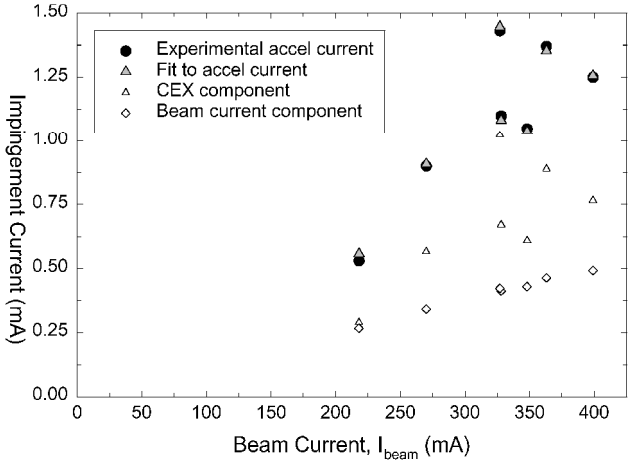

Fig. 3 Observed accelerator grid current of GS003 and results of the least squares fit.

with I_{beam} (Ref. 14). Judging from the negative sum of P_I and P_{I2} terms, CEX ions formed in the plume are apparently more likely to avoid capture by the decelerator as the beam current is increased.

The accelerator current data yields a good fit with just the two terms involving P_E and P_I. The results are plotted in Fig. 3, where the individual contributions of the two terms are also plotted. While the P_E term is sufficient to reproduce much of the variability of I_{acc}, the P_I term provides an increasing "baseline" linearly dependent on I_{beam}. Like the decelerator fit, the term corresponding to CEX with the background gas mattered little and the coefficient was zero to within 3 standard deviations. The origin of the P_I term is uncertain, but its functional dependence is not consistent with CEX.

In a preliminary analysis the empirical expression $\Delta I^E_{\text{acc}} \cong 1.5\Delta I_{\text{dec}}$ was utilized.[15] This expression was obtained from direct comparison of operating points 3 and 4 of Table 1, and the assumption that decelerator grid current derives entirely from CEX ions, to obtain an estimate for I^E_{acc}. The operating points of Table 1 were extrapolated to 100% utilization ($I_{\text{dec}} \to 0$) and an estimate for the remaining accelerator grid current produced by processes independent of charge exchange (PIE) was obtained from $I_{\text{acc}} - I^E_{\text{acc}}$. If the decelerator impingement probability of CEX ions decreases with I_{beam} as already discussed, this approach overestimates the rate at which the PIE contribution rises with beam current. In the more detailed analysis here, the P_I term accounts for the PIE ions, which increase linearly with beam current.

CEX ions formed in the intergrid region are much more likely to impinge on the accelerator grid than the decelerator because the accelerator grid potential is normally 175 V more negative (see Table 1). CEX ions formed downstream from the decelerator may strike its downstream face, but produce little erosion when they do so. The issue of downstream CEX trajectories and their relative probability of impinging on accelerator and decelerator grids is an important one, but beyond the scope of this study. However, experimental data concerning the rise in accelerator and decelerator current levels with background pressure are available and relevant. The T5 data, obtained with the BTS grid set, show the decelerator current rising nearly an order of magnitude faster than accelerator current.[12] Although the BTS decelerator thickness was 3 times greater and possibly more effective at screening the accelerator potential, this is strong evidence that the contribution of downstream CEX current to I_{acc} is minor. The adequacy of two terms to fit the data provides further support. In addition, a study of a 30 cm ion engine of entirely different grid design obtained comparable data concerning the effect of background pressure on I_{acc} and I_{dec} (Ref. 13).

Some of the CEX ions striking the accelerator grid will do so at an energy substantially exceeding 225 eV. This is because the CEX probability decreases with Xe^+ energy, so that CEX is more likely per unit time during the acceleration phase than the extraction phase. For example, a CEX ion formed when a xenon ion has traversed 50% of the screen–accelerator gap can impinge on the accelerator grid with an energy of about $0.50[1100 - (-225)] = 668$ eV. As a result, for a properly designed, properly operated extraction GS with accelerator/decelerator grid voltages of −225/−50, accelerator erosion rate is expected to dominate over decelerator erosion rate.

One possible origin of PIE ions below the perveance limit was considered to be the coulomb scattering of the ions. Impingement current due to such a process would depend on the square of beam current. Both coulomb and ion-neutral scattering were included in the modeling effort.

Performance of GS004

As already stated, GS004 and GS003 were fabricated according to the same design specifications, but GS003 had undergone a brief earlier period of testing. GS004 was operated at 25 mN (see Table 3) during the majority of the test period, which occupied portions of four successive days. Its initial performance at 22 mN was similar to GS003; however, both accelerator- and decelerator-grid current levels were quite high at the 25 mN operating point. The accelerator- and decelerator-grid currents were highly sensitive to adjustment of the accelerator voltage at 25 mN (see Table 3), indicating direct impingement on each grid by energetic ions. At a beam current of 457 mA, a reduction in discharge current on the third day of operation resulted in a substantial rise in both accelerator- and decelerator-grid current levels (see operating points 7 and 8). The reduced discharge current is compensated by increases in magnetic field strength and discharge voltage. Increased magnetic field strength improves electron confinement efficiency, whereas increased discharge voltage raises the Bohm velocity and electron energy. These effects help to compensate for a reduced ion production rate associated with decreased discharge current. The ratio Xe^{2+}:Xe^+ increases rapidly with discharge voltage.[14]

Table 3 Operating parameters for selected operating points, GS004[a]

Operating point	I_{beam}, mA	V_{anode}, V	I_{anode}, A	V_{acc}, V	I_{acc},[b] mA	I_{dec},[b] mA	$I_{\text{acc}} + I_{\text{dec}}$, mA	η_m, %
1	398	44.2	2.65	−225	1.27	0.36	1.63	——
2	457	42.0	2.65	−225	2.50	1.18	3.68	80.3
3[c]	456	42.2	2.65	−225	3.27	1.61	4.87	80.1
4	458	42.7	2.65	−175	4.81	2.20	7.01	80.5
5	458	42.1	2.65	−250	2.24	0.92	3.16	80.5
6	457	41.9	2.65	−225	2.47	1.13	3.60	80.3
7	457	40.7	3.00	−225	2.20	0.80	3.00	80.3
8	457	42.2	2.65	−225	2.64	1.13	3.77	80.3
BTS	457	43.5	3.00	−225	1.20	0.90	2.10	88.0

[a] $V_{\text{beam}} = 1100$ V and $V_{\text{dec}} = -50$ V.
[b] Absolute accuracy is ±10 μA.
[c] Cathode current set to 1.00 A rather than normal 0.65 A setting.

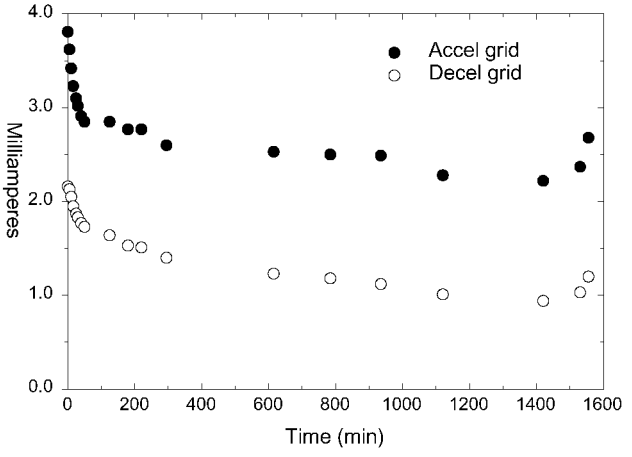

Fig. 4 Grid currents at the normal 25 mN operating point (see Table 2) during the four days of GS004 wear testing.

The effect of main cathode current on grid current levels is even more pronounced than discharge voltage. This accounts for the high grid currents of operating point 3, for which the cathode current was 1.00 A rather than 0.65, the normal setting. In conjunction with the higher cathode current setting, ΔV between cathode and keeper increased about 1.3 V, whereas V_{anode} increased only 0.4 V. Given the energy dependence of emitted ions on cathode current level measured in other studies,[16] the elevated grid currents of operating point 3 may result from an upward shift in the cathode ion energy distribution and flux level. The cathode ion flux will increase rapidly with cathode current,[17] and these ions by virtue of their high initial velocity and broad velocity distribution, assuming they arrive at the grids with these same initial properties, could have a greater probability of accelerator/decelerator grid impingement. Based on these considerations, the velocity distribution function for ions entering the extraction grids may be quite important in determining grid impingement currents. As far as we are aware, neither the width of this distribution nor the effects of ion–ion (coulomb) and ion-neutral scattering have been considered in previous ion engine models.

Figure 4 shows the grid currents observed during stable operation at the 25-mN operating point during most of the GS004 wear test. Grid currents during warmup and performance mapping are not shown. The trend is clearly down, except for an upward spike at about 1500 min. This spike was associated with increased recycling activity. The downward trend in grid current is consistent with previous BTS experience and is believed to arise from gradually increasing aperture size. This trend would be expected to continue over the course of several hundred hours of operation and beyond, with the slope gradually flattening.[2] The slope in Fig. 4 gets its large negative value as a result of thruster operation in the vicinity of the perveance limit, but after an extended run at such an operating point, BTS experience shows that accelerator impingement current is also reduced at operating points far from the perveance limit. CEX current will drop with enlargement of the accelerator-grid apertures because the product of neutral xenon density and beamlet ion flux decreases more rapidly than the increase of aperture cross-sectional area. The magnitude of this effect does not appear to be sufficient to explain observed results, however.

Modeling

Computer models of flow through ion grid apertures have been developed previously by Arakawa and Ishihara[18] and by Peng et al.[19] In Ref. 18, a particle description of the ions was employed. Neutral flow was neglected as was CEX. In Ref. 19, the ions were again treated using particles, but in this case CEX was included by assuming a constant neutral flowfield. In both Refs. 18 and 19, only single-charged ions were considered. In the present work, the ions and neutrals are treated in detail using a combination of two particle methods. The particle-in-cell method (PIC)[20] is employed to model the plasma dynamics. In the present study, ions (both single and double charges) are treated as particles. Following the work of Peng et al.[19] electrons are only assumed to exist in the region upstream of the screen grid. A fluid approach is employed for the electrons in which their temperature T_e is assumed to be constant, and their number density n_e is given by the Boltzmann relation:

$$n_e = n_{\text{ref}} \exp[(\phi - \phi_0)/T_e] \tag{2}$$

where ϕ_0 is about 1100 V. The reference density n_{ref} is taken to be the total ion charge density employed in the upstream boundary conditions (see subsequent discussion). The Poisson equation is solved on a rectangular grid, where the ion density is given by the particles and the electron number density is given by the above equation. Following the approach of Samanta Roy et al.[4] an alternating direction implicit method is employed to solve the Poisson equation, which is nonlinear due to the presence of ϕ in the preceding equation for the electron number density.

The second particle technique employed is the direct simulation Monte Carlo method (DSMC),[21] which is used to model collision phenomena. Thus, the neutral atoms are also treated as particles, and three different types of collisions are modeled: 1) momentum transfer using the cross sections of Dalgarno et al.,[22] 2) CEX between Xe and Xe^+ using the cross sections of Sakabe and Izawa[23] and between Xe and Xe^{2+} using the following curve fit to the measurements of Hasted and Hussain[24]:

$$\sigma = [3.4069 \times 10^{-9} - 2.7038 \times 10^{-10} \log(g)]^2 \text{ m}^2 \tag{3}$$

and 3) coulomb collisions. For coulomb collisions, the equations from classical plasma physics for cross section and scattering angle are employed (e.g., see Ref. 24). However, the scattering angle for a particular collision is sampled statistically from the distribution suggested by Nanbu.[25] This procedure is necessary because DSMC–PIC is a statistical approach and the method does not compute intersecting particle trajectories deterministically. In Fig. 5, a selection of the collision cross sections employed in the present study is shown for the xenon system as a function of relative velocity. It can be concluded that coulomb collisions dominate at low collision energies. At high energy, the CEX cross section dominates. In Fig. 6, the variation of coulomb scattering angle with relative velocity is shown. Here, it is evident that only very glancing interactions occur even at the low relative velocities that provide the largest cross sections (again see Fig. 5).

The upstream boundary conditions for the DSMC–PIC approach involve specification of species number densities, velocities, and temperatures. The temperature of the neutral atoms is assumed to be 500 K. The temperature of the ions is taken to be 4 eV based on a fit to the measurements of Pollard (see data of Ref. 14, Fig. 15). The electron temperature is not well known, and a value of 5 eV

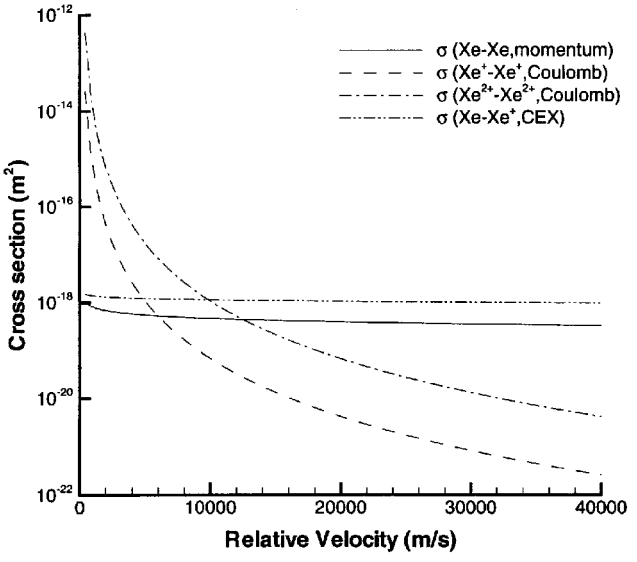

Fig. 5 Collision cross sections as function of relative velocity.

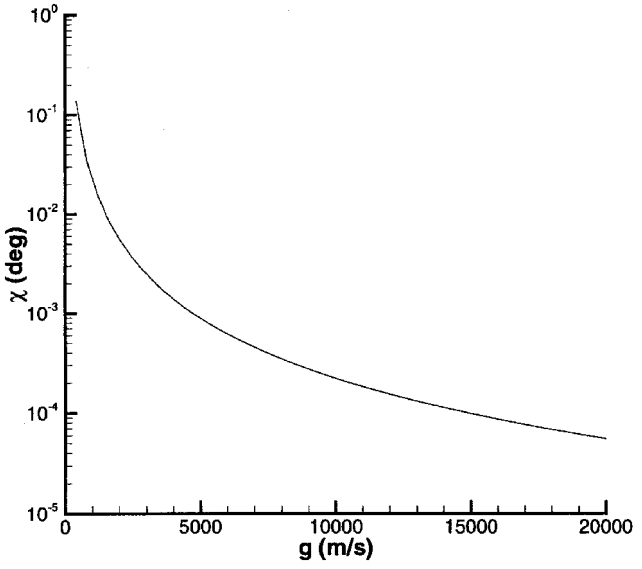

Fig. 6 Coulomb collision scattering angle as a function of relative velocity.

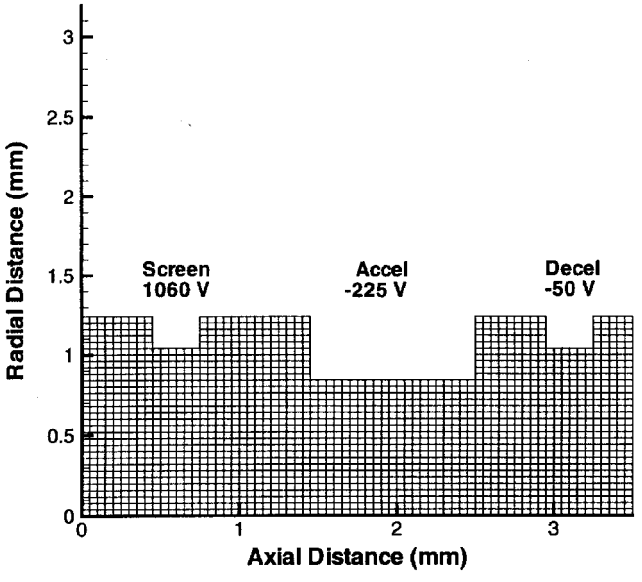

Fig. 7 Computational grid employed.

is assumed here. These temperatures are employed to calculate the atom and ion velocities of particles entering the flow domain from the discharge chamber. In each case, the flux of species i across a radial surface upstream of the screen grid is given by the standard result from kinetic theory:

$$\Gamma_i = \tfrac{1}{4} n_i C_i \tag{4}$$

where the mean molecular speed is given by

$$C_i = \sqrt{8kT_i/\pi m_i} \tag{5}$$

The atom and ion fluxes are computed so as to be consistent with the experimentally measured values of total beam current and propellant efficiency. Thus, through the use of Eq. (4), the atom and ion number densities are determined. One further parameter that cannot be determined from the measured systems parameters is the fraction of ions that are double charged. Based on the measurements of Pollard,[14] it is expected that current fraction lies between 0.05 and 0.20. Various values are employed in the computations.

The computational grid employed in all simulations is shown in Fig. 7. The cell size is less than the smallest Debye length considered in these investigations. The cell sizes are 40–50 μm, orders of magnitude smaller than the mean free paths for all flow conditions. The time step employed in the simulations falls in the range 0.1–0.4 ns and is the reciprocal of the plasma frequency. The surfaces of the three screens are at fixed potentials and are assumed to have a constant temperature of 500 K. Ions striking any of the screens are assumed to recombine to neutral atoms. The facility back pressure is sufficiently low such that it has virtually no effect on the flow through the screens. It is, therefore, neglected in the computations.

The main purpose of the computations is to predict the ion current to the acceleration grid. This is computed by directly counting the number of ion particles impacting on any surface of the acceleration grid over a finite period of physical time. The current collected by the deceleration grid is not considered here because an adequate treatment of the neutralized plasma downstream of the thruster exit plane is required. This is left for future study.

Computational Results

Six operating points of GS003 cataloged in Table 1 are investigated computationally, cases 1–3 and 5–7.

For each of these cases, three simulations are computed in which the fraction of double-charged ions is set to 0.0, 0.1, and 0.2. In addition, further computations are performed for cases 3 and 7 to assess the sensitivity of the solutions to the value of the electron temperature assumed and to test the effect of the different types of collisions.

In Fig. 8, contours of plasma potential are shown for a computation of case 3 with 10% double-charged ions. These have the expected shape seen in previous computational studies,[18,19] which result in the ions first being accelerated away from the screen grid and finally pulled up toward the acceleration and deceleration grids.

In Fig. 9, the variation of current collected on the acceleration grid as a function of total beam current is shown. The experimental accuracy of the grid current is ± 10 μA. The computational results indicate a sensitivity to the fraction of double-charged ions assumed in the discharge plasma. It is found that higher fractions of Xe^{2+} lead to smaller current being collected on the acceleration grid. Close examination of the computational results revealed the explanation for this phenomenon. When there is a significant fraction of Xe^{2+} in the plasma, the average ion velocity is increased because the electric fields accelerate the double-charged ions to higher velocities than the single-charged ions. In terms of the current collected by the acceleration grid, this effect is most important in the region next to the screen grid, where the ions are accelerated by the potential gradients in the direction toward the centerline of the aperture. Hence, in the case where there is a finite fraction of Xe^{2+}, more of the plasma is accelerated toward the centerline in comparison to the case where there is no Xe^{2+}.

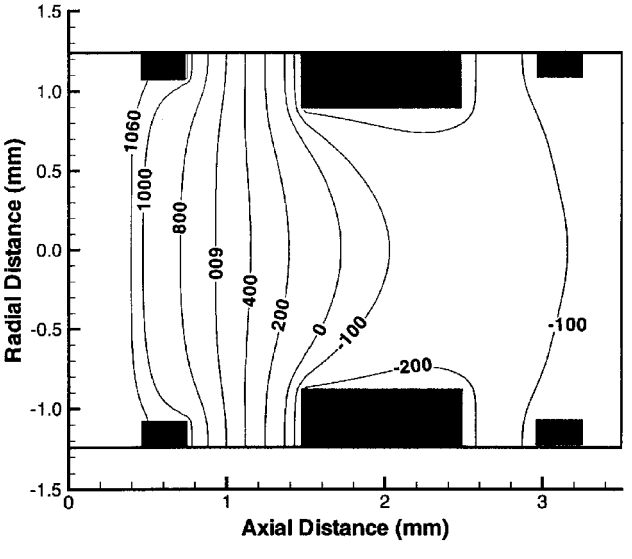

Fig. 8 Contours of plasma potential for case 3.

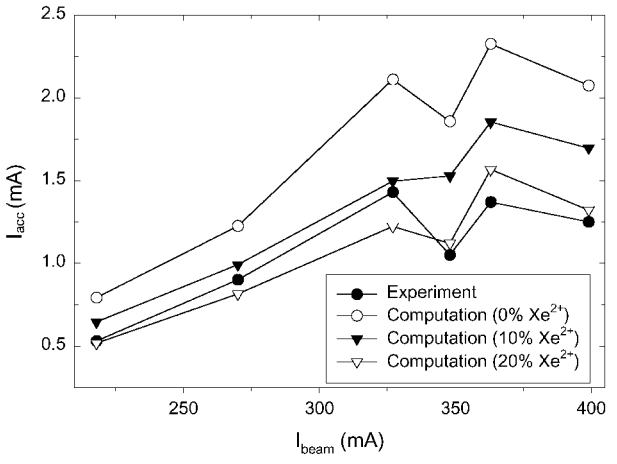

Fig. 9 Variation of current collected on accelerator grid as a function of total beam current.

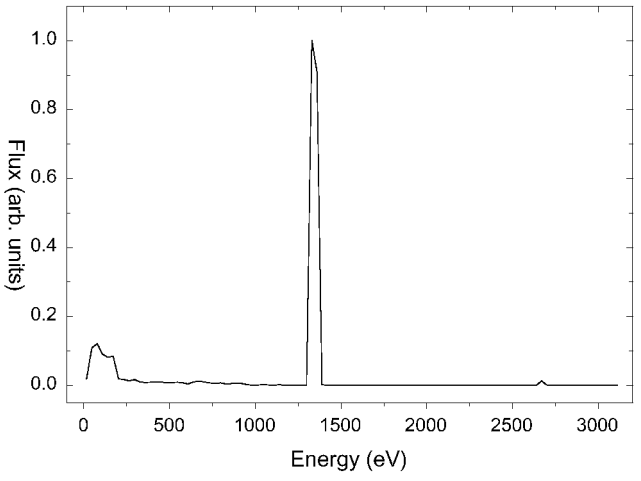

Fig. 10 Computed energy spectrum of the accelerator ion impingement for case 3, with 10% Xe^{2+}.

Returning to the data shown in Fig. 9, in general, the computational results using 20% of ions having double charge offer good agreement with the experimental data at high V_{anode} settings, ≈43–45 V. At the lower V_{anode} settings, the experimental data are usually found above the 20% double-charge computational results, in good agreement with the 10% case. These values are consistent with the general trend, not absolute values of multiple-charged ion fractions as a function of thruster operation conditions reported by Pollard.[14] The $I_{beam} = 363$ mA operating point is an exception, with the expected I_{acc} significantly below the trends considering the relatively low V_{anode} value of 38.9 V.

The computational results shown in Fig. 9 include all collision mechanisms and employ an electron temperature of 5 eV. Further computations indicated that omission of the CEX collisions leads to a reduction in the accelerator grid current by values lying between 15 and 45% depending on the specific conditions. Omission of the coulomb collisions has no effect on the current collected. For operating point 3, increasing the electron temperature to 10 eV decreased the current collected by 23%. For the same case, decreasing the electron temperature to 4 eV increased the acceleration-grid current by 13%. These results are because ϕ, the local plasma potential, is directly proportional to the electron temperature. This is clearly seen by inverting the Boltzmann relation of Eq. (2). Because in our model T_e is a constant, the spatial derivatives of potential (that is, the electric fields) are also proportional to the electron temperature. At higher electron temperature, there is a greater acceleration of ions away from the screen grid than is simulated at lower electron temperature. Thus, as the electron temperature is increased, there is a decrease in current collected on the acceleration grid.

The calculated energy spectrum of ions impinging on the accelerator grid, for case 3 with 10% Xe^{2+}, is plotted in Fig. 10. The dominant peak is Xe^{+} centered at $V_{beam} - V_{acc}$. A very small Xe^{2+} feature occurs at twice this value. These peaks are produced by the PIE ions. The impingement flux of CEX ions has a broad feature below 250 eV and a tail on the high-energy side. In terms of flux contributions, 28% of the impingement current derives from CEX ions and 0.5% from Xe^{2+}. The rest is due to PIE ions. Even before factoring in the increased sputter yield with impingement energy, this result predicts that most of the accelerator grid erosion is produced by Xe^{+} ions at a kinetic energy determined by $V_{beam} - V_{acc}$, with CEX playing a minor role. For comparison, the P_E term-representing the CEX associated with the source flow-accounts for about 71% of the total observed I_{acc} (see Fig. 3). It is possible that the model underestimates the CEX current because it does not include ions that originate downstream from the decelerator grid and migrate upstream to the accelerator grid. We have already presented evidence that the downstream ions are a minor contributor, but including such ions may improve agreement between the experimental results and theoretical predictions. In addition, the selected ion temperature was a bit high and the radial variations of ion flux and utilization across the grids are not accurately known, and were neglected in the model. Finally, it should be noted that I_{acc} dependencies on f_{2+} and η_c are correlated. The fit to experimental data ignores the lower impingement probability of Xe^{2+}, which tends to cause an overestimate of the magnitude of the P_E term.

Although the agreement obtained between experiment and computation as shown in Fig. 9 is good, there is some level of uncertainty in the simulation results particularly in terms of specifying the discharge plasma parameters of electron temperature, ion temperature, and fraction of double-charged ions.

Discussion

The density of neutral xenon in the intergrid region and thruster near-field is dominated by the density of the source flow rather than the density of background gas. A few mm downstream from the decelerator the computed source flow density is 5×10^{11} cm^{-3} for case 7, whereas background density is about 6×10^{10} cm^{-3}. The density between screen and accelerator grids is typically about 2×10^{12} cm^{-3}. From the neutral density, grid geometry, and CEX cross sections, it is apparent that intergrid CEX cannot readily account for the observed I_{acc}. Other mechanisms of current production, including the photoelectric effect associated with the impingement of short-wavelength photons from the discharge, also appear too small in magnitude. However, the experimental data can be reproduced quite well upon assuming that ions have a radial velocity distribution during extraction that is consistent with an ion temperature of 4 eV, and reducing this would improve the agreement.

All of the previous modeling studies of ion engine plasma and ion extraction appear to have assumed ion temperature similar to neutral atom or wall temperature, far below the electron temperature. Similarly, ion temperature was not determined in the Langmuir probe study of the discharge chamber, and it was thought to be two orders of magnitude below T_e (Ref. 26).

Recently, experimental and theoretical evidence has become available indicating that the ion temperature in low-density plasmas can be very substantial. Numerical models of plasma jet propagation for the stationary plasma thruster have utilized ion temperatures between 4 and 40 eV to reach agreement with experiment.[27,28] Some recent studies of plasma reactors and the ion etching process have found ion temperature to be far above the wall temperature.[29,30]

Because of the potential gradient[26] in the discharge chamber and the need for high ion migration rates to the screen grid during thruster operation, most ions may be expected to have kinetic energies of 1–5 eV at the time they encounter the plasma sheath. This kinetic energy will have a radial component as well as an axial component, because the screen grid and discharge wall are at the same potential and both radial and axial potential gradients exist.[26] Whereas the T5 far-field measurement of ion energy distribution[14] is consistent with an ion temperature of 4 eV, direct measurements of the ion velocity distribution and other properties inside the discharge plasma and

intergrid regions would be valuable. The radial velocity distribution may be less energetic than the axial distribution.

There is the further issue of whether the ion radial velocity distribution is the same in the intergrid region as in the discharge chamber, and even whether it is axially symmetric within a given grid aperture. While it has to be symmetric at the grid center for a cylindrically symmetric thruster, for apertures away from the axis of symmetry most ions are expected to approach on the side nearest the grid center. This is due to the radial potential gradient and distribution of plasma in the discharge chamber. With a non-symmetric and off-normal distribution of ion trajectories into a screen aperture (relative to the axis of symmetry of a given screen-accelerator-decelerator combination of apertures), the radial velocity distribution may be large and non-axially symmetric even after the ions are accelerated. If this is the case, ion temperature as high as 4 eV is not required to obtain high radial ion velocities during extraction.

The PIE current may depend on various parameters of the discharge plasma, shape of the plasma sheath associated with individual screen grid apertures, geometry, and extraction voltages of the extraction grid set. PIE ions will impinge at high energy and produce much more erosion and grid damage per ion than typical CEX ions. Given this and the possible influence of PIE ions in previous studies of accelerator-grid erosion, prior experimental and theoretical work on accelerator-grid wear may need to be reevaluated for all ion engines. Performance characteristics that may imply a significant role for PIE ions include extrapolation to nonzero erosion rate or nonzero I_{acc} at $\eta_c = 100\%$, scattering in the plot of I_{acc} vs $(1-\eta_c)FI_{beam}(1-f_{2+}/2)P_E$, nonlinear dependence of grid erosion rate on accelerator-grid voltage, and low fractional change in erosion rate or grid current with background pressure or η_c.

Inspection of results for other thrusters[31,32] suggests that grid impingement of non-CEX ions may be of general importance for ion engines. The fit of Eq. (1) to I_{acc} for the 30-cm NSTAR ion engine (see Ref. 32 for data; see Fig. 11 and Table 2 for fit results) has typical residuals greater than 100 μA using all 5 parameters, and several hundred μA for the best 3-parameter case. The value of f_{2+} had been measured at each operating point[32] so that η_c was accurately known. The P_{I2} term was the largest contributor (see Fig. 11). Source and background CEX terms had little effect on the quality of fit, with each term zero to within a standard deviation. The source term was of greater importance to the fit, but its coefficient was negative (see Table 2 and Fig. 11). The reason for a negative value is obvious from a comparison of the two operating points at $I_{beam} = 1760$ mA with $\eta_m = 0.89$ and 0.94 (see Table 1 of Ref. 32). I_{acc} is different at these points by about 9%, with $\Delta I_{acc}/\Delta\eta_c$ having the wrong sign if CEX impingement accounts for I_{acc}. Differences in V_{anode} and I_{anode} at the 1760 mA operating points are below 10%, but the cathode flow rate is 23% higher for the case with lower values of I_{acc} and η_m. The energy, charge state distribution, and flux of ions from the hollow cathode might be a factor here in determining the I_{acc} levels. Using P_E and P_{EB}, or P_I and P_{I2} terms of Eq. (1), the general upward trend of I_{acc} can be readily obtained but considerable scatter of data points is inevitably present. Clearly, CEX in itself is not providing an adequate explanation of the observed I_{acc} of the NSTAR thruster.

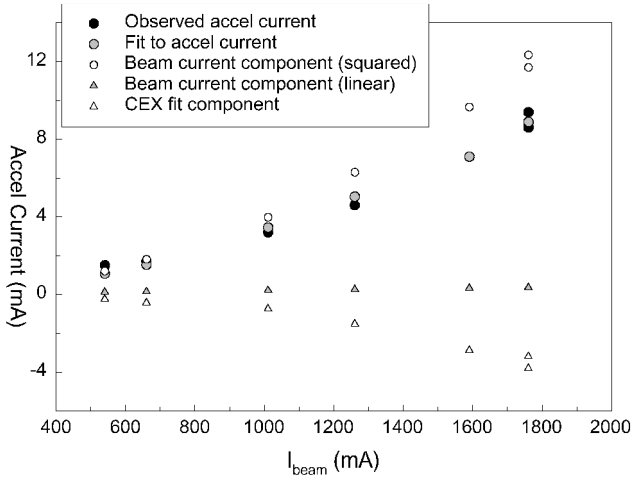

Fig. 11 Observed accelerator grid current for the 30-cm NSTAR ion thruster (data from Ref. 32), and results of the least squares fit.

The effect of PIE ions may be substantial despite the relatively low NSTAR discharge voltage, ≈26 vs ≈40 V for the T5. The 90+% utilization (η_m) results in low impingement rates by CEX ions. In addition, the larger grid diameter (30 vs 10 cm) will reduce the total production rate of CEX ions by a factor of about 9 at a given flow rate, utilization, and beam current, in the region just downstream from the grids. Because the accelerator aperture diameter is only 1.1 mm at the NSTAR beginning of life, the total inter-grid CEX production rate for NSTAR (same F, η_c, and I_{beam} as in the T5 case) is lower by a smaller factor than 9. The low CEX production rate may increase the fraction of I_{acc} corresponding to PIE ions at the lower I_{beam} settings. Even allowing for the collection of more CEX ions from downstream because of the elimination of the decelerator grid, the 1.5 mA of accelerator current at the lowest NSTAR beam current setting of 540 mA seems high. Scaling the sum of accelerator and decelerator current for the T5 operating point $I_{beam} = 399$ mA according to F, I_{beam}, η_c and grid geometry leads to a substantially lower figure than observed, providing further confirmation that NSTAR I_{acc} is not 100% CEX impingement. A tentative conclusion was reached in the analysis of the NSTAR lifetest that the accelerator impingement energy or sputter yield was one-fourth the published value for molybdenum.[32]

CEX production in the source flow will increase according to the square of I_{beam} at constant utilization, but the NSTAR I_{acc} dependence on I_{beam} was between first and second order, and the exponent seems to increase with I_{beam}. The observed wear pattern on the NSTAR accelerator grid indicates that CEX impingement on the downstream face is an important erosion mechanism at the nominal operating point. The 2 mA reduction in I_{acc} during the first 2000 h of operation and the large increase in accelerator aperture diameter over the duration of the NSTAR lifetest are consistent with a non-CEX erosion mechanism.

For the NSTAR case, V_{anode} was nearly constant while I_{anode} was varied to obtain the desired I_{beam}, suggesting that I_{anode}, like V_{anode}, may have considerable influence on I_{acc}. This is indicated also by the comparison of operating points 7 and 8 of GS004 (where I_{anode} settings differ and V_{anode} was free to adjust, see Table 2). However, here the thruster is at the perveance limit and the sign of $\Delta I_{acc}/\Delta V_{anode}$ is opposite to the normal result, indicating that the effect of Xe^{2+} fraction on I_{acc} becomes minor compared to the effect of another parameter, perhaps the ion radial velocity distribution, at the perveance limit.

Decelerator current for GS003 is dominated by CEX ions over the range of operating points in Table 1, whereas accelerator current also has a large contribution from PIE ions. PIE ion impingement will primarily erode accelerator grid barrels, whereas CEX ions may erode the grid face as well and, on twin GS, produce pit and groove features. In comparison to the accelerator grid, the decelerator-grid aperture is considerably larger (see Fig. 7), which may reduce its collection of PIE ions.

Both impingement and erosion rate can readily be dominated by CEX ions at low utilization, when the accelerator-grid operating voltage is at high absolute value.[12] The effects of PIE ions are likely to dominate at high utilization with a low absolute voltage on the accelerator grid.

Conclusions

This study purports to show that CEX ions do not fully account for the collected extraction grid current in ion thrusters. The result is of considerable potential importance for the improvement of ion engine lifetime and reduction of contamination effects because it may be possible to tailor grid set and/or discharge chamber design to reduce ion impingement and its associated grid erosion. Although the agreement between theory and experiment is better for this more detailed treatment than for previous modeling studies, a number of uncertainties remain to be resolved. In addition, the

experimental data suggest a greater role for CEX ions than the model predicts.

The use of flight-model grids was essential for this study. Previous T5 GS were inadequate for study of impingement current because of the inferior grid concentricity and direct impingement commonly collected by the decelerator grid. The performance of the flight-model grids was very good, with accelerator and decelerator impingement current as low as 0.24 and 0.10%, respectively, of the beam current. This is comparable to the accelerator grid to beam current ratio of the NSTAR thruster at similar beam current levels, despite the lower propellant utilization of the T5 thruster and its smaller size.

The Xe^+ flux at ion beam energy is known to drop by roughly an order of magnitude per 10-deg angular rotation away from the thrust axis, in the far field, with no sharp discontinuities. This behavior is qualitatively consistent with the influence of various scattering processes or a radial ion velocity distribution far more energetic than the wall temperature of the discharge chamber would produce. Scattering effects were found to be minor in this study.

The variation of accelerator grid current levels with propellant mass utilization and parameters of the discharge is inconsistent with the accepted view that the current is entirely due to CEX ions. The collected T5 grid currents have been attributed to two main sources, one of which is determined by the details of CEX ion formation and migration, and the other by PIE. Both sources are important for the accelerator grid, whereas decelerator-grid current was interpreted in terms of CEX ions only. In addition, double-charge ions were found to have a low impingement probability, so that changes in the charge state ratio significantly affect the collected accelerator grid current.

At the operating points of this study, PIE ions may dominate the erosion of the accelerator grid. The erosion by PIE ions should be self limiting to a degree because the enlargement of accelerator apertures will tend to slow the erosion rate if the screen apertures remain constant. The production of CEX ions will also decrease with aperture enlargement. These observations are expected to account for the downward, gradually flattening trend of collected accelerator-grid current and recorded QCM mass gain over long periods of thruster operation.

Acknowledgments

The preparation of this manuscript was supported in part by The Aerospace Corporation through an Independent Research and Development Program. The authors wish to thank the Defence Evaluation and Research Agency for providing the grid sets, and N. Wallace, D. Mundy, P. Wheldon, and H. Simpson for their efforts during the data collection phase of April–May 1996 at The Aerospace Corporation. A. Shagayda, D. G. Fearn, and J. E. Pollard provided useful discussion. Figure 1 was supplied by D. Mundy.

References

[1]Brophy, J. R., Polk, J. E., and Rawlin, V. K., "Ion Engine Service Life Validation by Analysis and Testing," AIAA Paper 96-2715, July 1996.

[2]Crofton, M. W., "Evaluation of the United Kingdom Ion Thruster," *Journal of Spacecraft and Rockets*, Vol. 33, No. 5, 1996, pp. 739–747.

[3]Fearn, D. G., "Ion Thrusters Lifetime Limitations Imposed by Sputtering Processes," *Proceedings of the 23rd International Electric Propulsion Conference*, Paper 93-177, Sept. 1993.

[4]Samanta Roy, R. I., Hastings, D. E., and Gatsonis, N. A., "Ion-Thruster Plume Modeling for Backflow Contamination," *Journal of Spacecraft and Rockets*, Vol. 33, No. 4, 1996, pp. 525–534.

[5]Kitamura, S., Hayakawa, Y., Kasai, Y., and Ozaki, T., "Fabrication of Carbon–Carbon Composite Ion Thruster Grids—Improvement of Structural Strength," *Proceedings of the 25th International Electric Propulsion Conference*, Paper 97-093, Aug. 1997.

[6]Shimada, S., Satoh, K., Gotoh, Y., Nishida, E., Noro, T., Takegahara, H., Nakamaru, K., and Nagano, H., "Ion Thruster Endurance Test Using Developmental Model Thruster for ETS-VI," *Proceedings of the 23rd International Electric Propulsion Conference*, Paper 93-169, Sept. 1993.

[7]Polk, J. E., Anderson, J. R., Rawlin, V. K., Patterson, M. J., and Sovey, J., "In Situ, Time-Resolved Accelerator Grid Erosion Measurements in the NSTAR 8000 Hour Ion Engine Wear Test," *Proceedings of the 25th International Electric Propulsion Conference*, Paper 97-047, Aug. 1997.

[8]Tartz, M., Hartmann, E., Deltschew, R., and Neumann, H., "Grid Erosion Study of a Three-Grid Ion Thruster," AIAA Paper 98-3646, July 1998.

[9]Shutthanandan, V., Ray, P. K., Shivaparan, N. R., Smith, R. J., Thevuthasan, S., and Mantenieks, M. A., "On the Measurement of Low-Energy Sputtering Yield Using Rutherford Backscattering Spectrometry," *Proceedings of the 25th International Electric Propulsion Conference*, Paper 97-069, Aug. 1997.

[10]Brophy, J. R., Pless, L. C., and Garner, C. E., "Ion Engine Endurance Testing at High Background Pressures," AIAA Paper 92-3205, July 1992.

[11]Crofton, M. W., "Laser Spectroscopic Study of the T5 Ion Thruster," AIAA Paper 95-2921, July 1995.

[12]Ahmed, L. N., and Crofton, M. W., "Surface Modification Measurements in the T5 Ion Thruster Plume," *Journal of Propulsion and Power*, Vol. 14, No. 3, 1998, pp. 336–347.

[13]Brophy, J. R., Garner, C. E., Goodfellow, K. D., Pivirotto, T. J., and Polk, J. E., "Electric Propulsion System Technology," Jet Propulsion Lab., Annual Rept. 1991, No. 92-10, California Inst. of Technology, Pasadena, CA, Nov. 1992.

[14]Pollard, J. E., "Plume Angular, Energy, and Mass Spectral Measurements with the T5 Ion Engine," AIAA Paper 95-2920, July 1995.

[15]Crofton, M. W., and Boyd, I. D., "The Origins of Accelerator Grid Current: Analysis of T5-Grid Test Results," AIAA Paper 99-2443, June 1999.

[16]Friedly, V. J., and Wilbur, P. J., "High Current Hollow Cathode Phenomena," *Journal of Propulsion and Power*, Vol. 8, No. 3, 1992, pp. 635–643.

[17]Crofton, M. W., "Preliminary Mass Spectrometry of a Xenon Hollow Cathode," *Journal of Propulsion and Power*, Vol. 16, No. 1, 2000, pp. 157–159.

[18]Arakawa, Y. and Ishihara, K., "A Numerical Code for Cusped Ion Thrusters," *Proceedings of the International Electric Propulsion Conference*, Paper 91-118, Oct. 1991.

[19]Peng, X., Keefer, D., and Ruyten, W., "Plasma Particle Simulation of Electro-Static Ion Thrusters," *Journal of Propulsion and Power*, Vol. 8, No. 2, 1992, pp. 361–366.

[20]Birdsall, C. K., and Langdon, A. B., *Plasma Physics via Computer Simulation*, Adam Hilger, Bristol, England, U.K., 1991, p. 479.

[21]Bird, G. A., *Molecular Gas Dynamics and the Direct Simulation of Gas Flows*, Oxford Univ. Press, Oxford, England, U.K., 1994, p. 458.

[22]Dalgarno, A., McDowell, M. R. C., and Williams, A., "The Mobilities of Ions in Unlike Gases," *Proceedings of the Royal Society*, Vol. 250, 1958, pp. 411–425.

[23]Sakabe, S., and Izawa, Y., "Simple Formula for the Cross Sections of Resonant Charge Transfer Between Atoms and Their Ions at Low Impact Velocity," *Physical Review A*, Vol. 45, No. 3, 1992, pp. 2086–2089.

[24]Hasted, J. B., and Hussain, M., "Electron Capture by Multiply Charged Ions," *Proceedings of the Physical Society*, London, Vol. 83, 1964, pp. 911–924.

[25]Nanbu, K., "Theory of Cumulative Small-Angle Collisions in Plasmas," *Physical Review E*, Vol. 55, No. 4, 1997, pp. 4642–4652.

[26]Masek, T. D., "Plasma Properties and Performance of Mercury Ion Thrusters," *AIAA Journal*, Vol. 9, No. 2, 1971, pp. 205–212.

[27]Boyd, I. D., "Computation of the Plume of the D55 Hall Thruster," AIAA Paper 98-3798, July 1998.

[28]Bishaev, A. M., Kalashnikov, V. K., Kim, V., and Shavykina, A. V., "Numerical Modeling of the Propagation of a Plasma Jet Produced by a Stationary Plasma Thruster in a Low-Pressure Gas," *Plasma Physics Reports*, Vol. 24, No. 11, 1998, pp. 923–928.

[29]Lymberopoulos, D. P., Wise, R. S., Economou, D. J., and Bartel, T. J., "Ion Density and Temperature Distributions in an Inductively Coupled High-Plasma Density Reactor," *IEEE Transactions on Plasma Science*, Vol. 24, No. 1, 1996, pp. 129, 130.

[30]Zheng, J., Brinkmann, R. P., and McVittie, J. P., "The Effect of the Presheath on the Ion Angular Distribution at the Wafer Surface," *Journal of Vacuum Science Technology A*, Vol. 13, No. 3, 1995, pp. 859–864.

[31]Gaeta, C. J., Matossian, J. N., Turley, R. S., Beattie, J. R., Williams, J. D., and Williamson, W. S., "Erosion Rate Diagnostics in Ion Thrusters Using Laser-Induced Fluorescence," *Journal of Propulsion and Power*, Vol. 9, No. 3, 1993, pp. 369–376.

[32]Polk, J. E., Anderson, J. R., Brophy, J. R., Rawlin, V. K., Patterson, M. J., Sovey, J., and Hamley, J., "An Overview of the Results from an 8200 Hour Wear Test of the NSTAR Ion Thruster," AIAA Paper 99-2446, June 1999.